



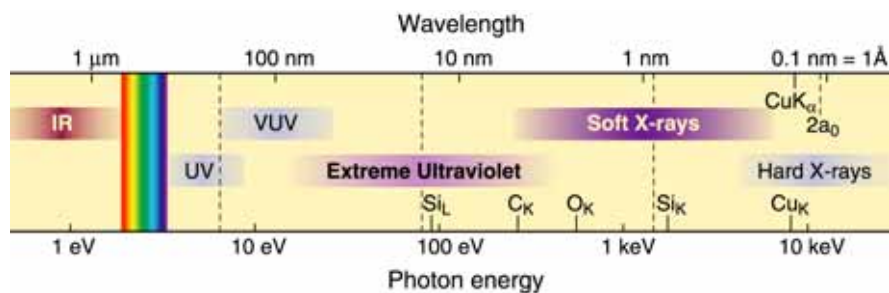
Soft and Hard X-Ray Microscopy

David Attwood
University of California, Berkeley

Cheiron School
September 2012
SPring-8

CheironSchool_Sept2012_Lec3.ppt 1

The short wavelength region of the electromagnetic spectrum



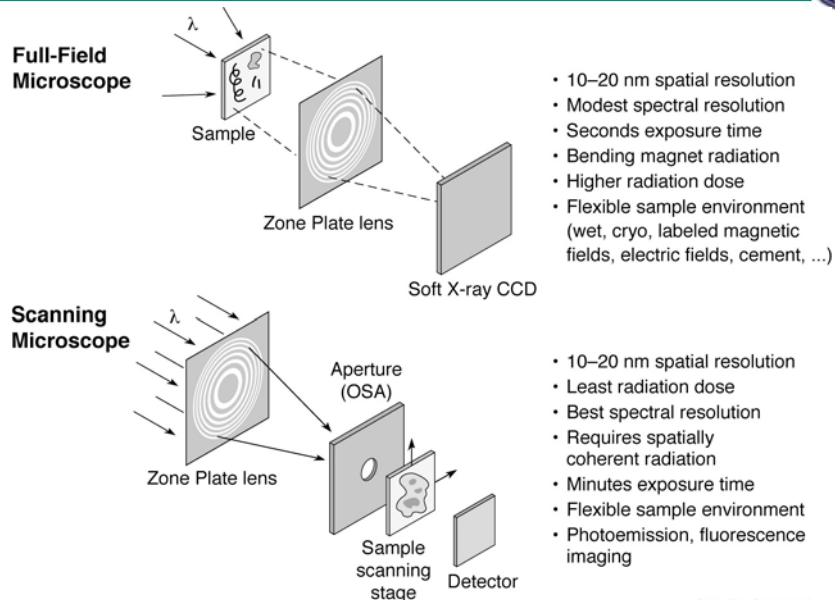
- See smaller features
- Write smaller patterns
- Elemental and chemical sensitivity

$$\hbar\omega \cdot \lambda = hc = 1239.842 \text{ eV nm}$$


$$n = 1 - \delta + i\beta \quad \delta, \beta \ll 1$$

CheironSchool_Sept2012_Lec3.ppt 2


Two common soft x-ray microscopes



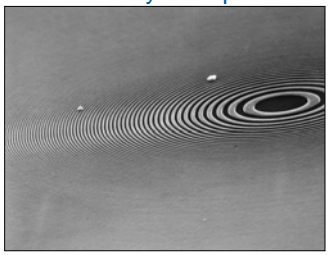
Ch09_F21_Sept2010.ai
CheironSchool_Sept2012_Lec3.ppt 3



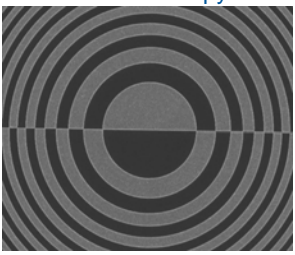
Novel diffractive optics



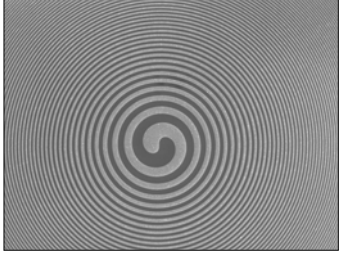
Soft x-ray zone plate



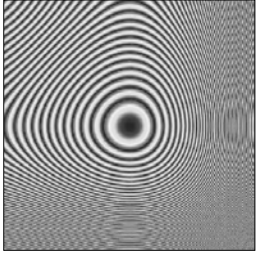
DIC microscopy



Spiral zone plate for phase contrast




Cubic phase plate for DOF



Courtesy of Anne Sakdinawat, Chang Chang, Weilun Chao and Erik Anderson (LBNL & UCB.)

CheironSchool_Sept2012_Lec3.ppt 4




Nature

LETTERS

Soft X-ray microscopy at a spatial resolution better than 15 nm

Weilun Chao^{1,2}, Bruce D. Harteneck¹, J. Alexander Liddle¹, Erik H. Anderson¹ & David T. Attwood^{1,2}



Analitical tools that have spatial resolution at the nanometre scale are indispensable for the life and physical sciences. It is desirable that these tools also permit elemental and chemical identification on a scale of 10 nm or less, with large penetration depths. A variety of techniques^{1–5} in X-ray imaging are currently being developed that may provide these combined capabilities. Here we report the achievement of sub-15-nm spatial resolution with a soft X-ray microscope—and a clear path to below 10 nm—using an overlay technique for zone plate fabrication. The microscope covers a spectral range from a photon energy of 284 eV (λ = 4.3 nm wavelength) to 1.8 keV (λ = 0.7 nm), so that primary K and L atomic resonances of elements such as C, N, O, Al, Fe, Cu and Ni can be probed. This X-ray microscopy technique is therefore suitable for a wide range of studies: biological imaging in the water window^{6,7}; studies of wet environmental samples^{8,9}; studies of magnetic nanostructures with both elemental and spin-orbit sensitivity^{10,11}; studies that require viewing through thin windows, coatings or substrates (such as buried electronic devices in a silicon chip¹²); and three-dimensional imaging of cryogenically fixed biological cells¹³.

The microscope XM-1 at the Advanced Light Source (ALS) in Berkeley¹⁴ is schematically shown in Fig. 1. The microscope type is similar to that pioneered by the Göttingen/BESS group (ref. 18, and references therein). A 'micro' zone plate (MZP) projects a full-field image to an X-ray sensitive CCD (charge-coupled device), typically in one or a few seconds, often with several hundred images per day. The field-of-view is typically 10 μm, corresponding to a magnification of 2,500. The condenser zone plate (CZP), with a central stop, serves two purposes in that it provides partially coherent hollow-cone illumination¹⁵, and, in combination with a pinhole, serves as the

$\lambda = 1.52 \text{ nm (815 eV)}$
 $\Delta r = 15 \text{ nm}$
 $N = 500$
 $D = 30 \mu\text{m}$
 $f = 300 \mu\text{m}$
 $\sigma = 0.38$
 $0.8 \Delta r = 12 \text{ nm}$

monochromator. Monochromatic radiation of $\lambda/\Delta\lambda = 500$ is used. Both zone plates are fabricated in-house, using electron beam lithography¹⁶.

The spatial resolution of a zone plate based microscope is equal to $1.22\lambda/NA_{MZP}$, where λ is the wavelength, NA_{MZP} is the numerical aperture of the MZP, and k_1 is an illumination dependent constant, which ranges from 0.3 to 0.61. For a zone plate lens used as high magnification, $NA_{MZP} = \lambda/2\Delta r_{MZP}$, where Δr_{MZP} is the outermost (smallest) zone width of the MZP¹⁷. For the partially coherent illumination^{15,16} used here, $k_1 = 0.4$ and thus the theoretical resolution is $0.8\lambda_{MZP}$, as calculated using the SPLAT computer program¹⁸ (a two-dimensional scalar diffraction code, which evaluates partially coherent imaging). In previous results with a $\Delta r_{MZP} = 23 \text{ nm}$ zone plate, we reported¹⁹ an unambiguous spatial resolution of 20 nm. Here we describe the use of an overlay nanofabrication technique that allows us to fabricate zone plates with finer outer zone widths, to $\Delta r_{MZP} = 15 \text{ nm}$, and to achieve a spatial resolution of below 15 nm, with clear potential for further extension.

This technique overcomes nanofabrication limits due to electron beam broadening in high feature density patterning. Beam broadening results from electron scattering within the recording medium (resist), leading to a loss of image contrast and thus resolution for

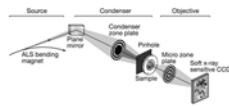
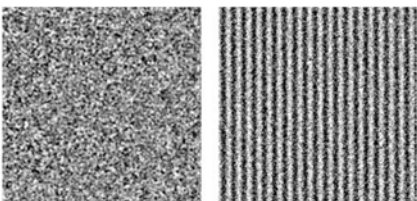



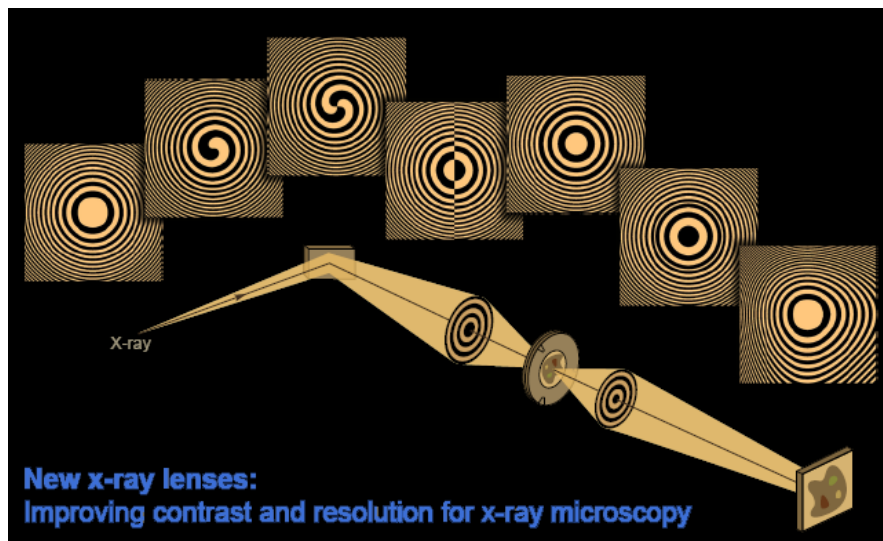
Figure 1 | A diagram of the soft X-ray microscope XM-1. The microscope uses a micro zone plate to project a full-field image onto a CCD camera that is sensitive to soft X-rays. Partially coherent, hollow-cone illumination of the sample is provided by a condenser zone plate. A central stop and a pinhole provide monochromatization.

Source: Soft X-ray Optics, Lawrence Berkeley National Laboratory, 1 Cyclotron Road, MS 2-002, Department of Electrical Engineering, California, Berkeley, California 94720, USA.

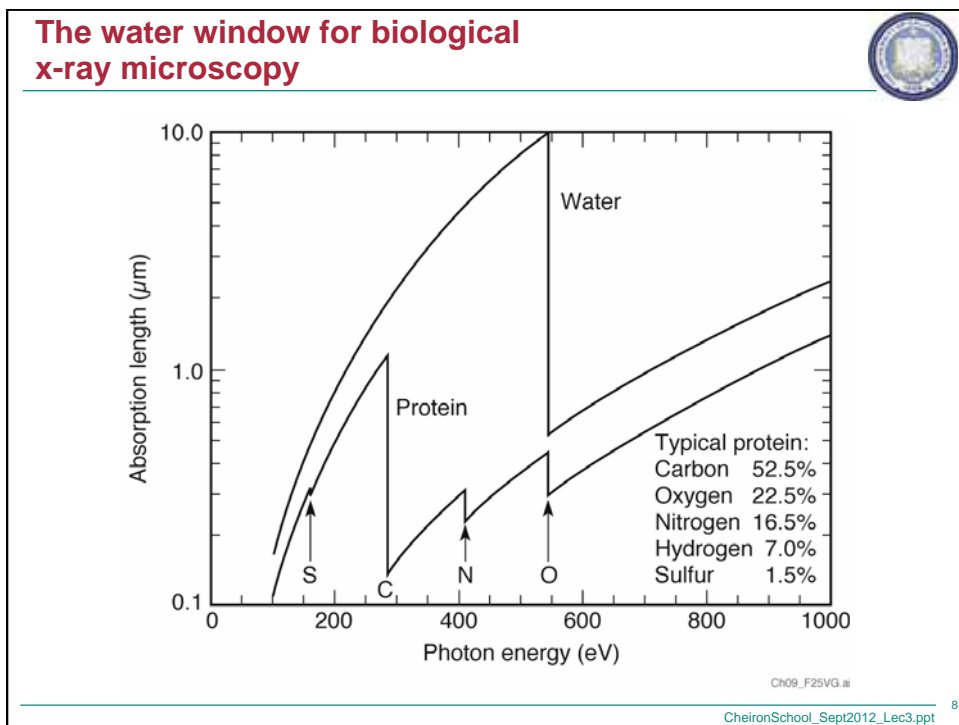
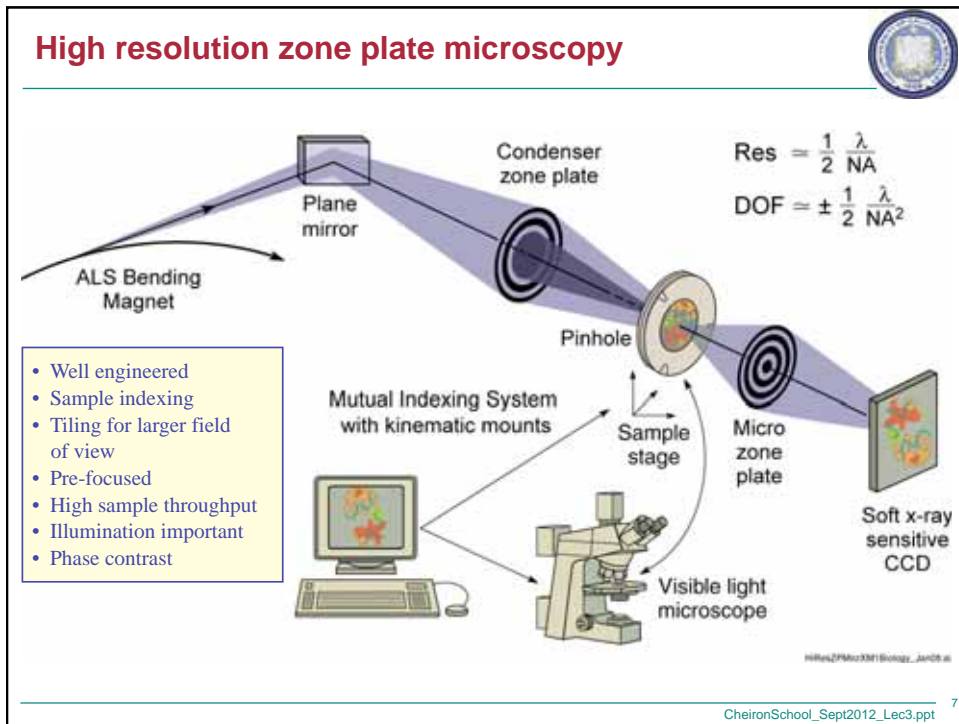
Figure 4 | Soft X-ray images of a 15.1 nm half-period test object, as formed with zone plates having outer zone widths of 25 nm and 15 nm.

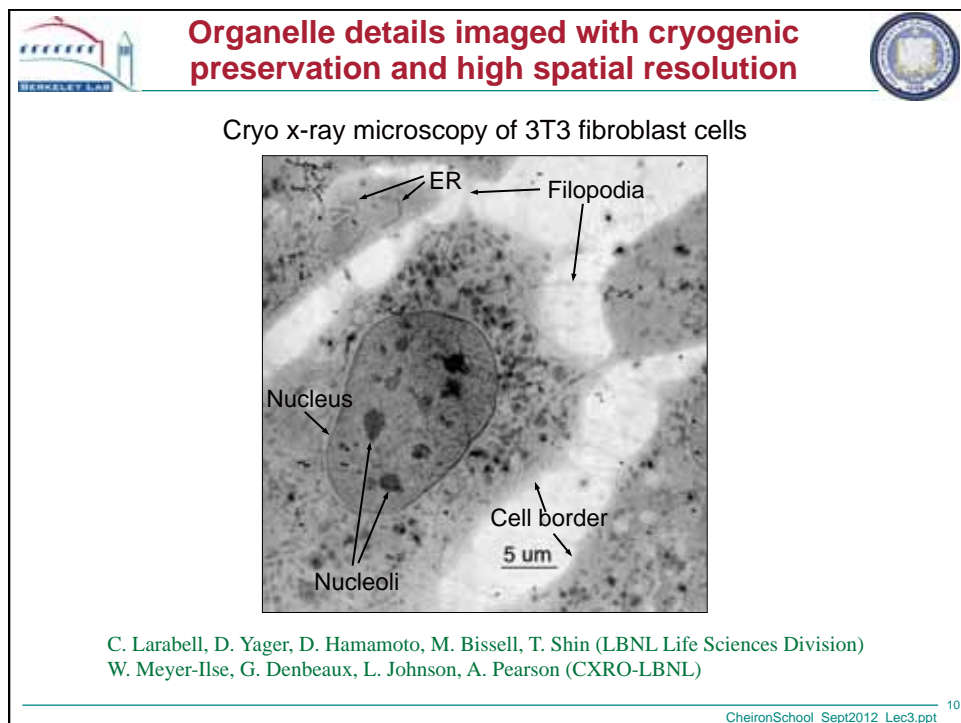
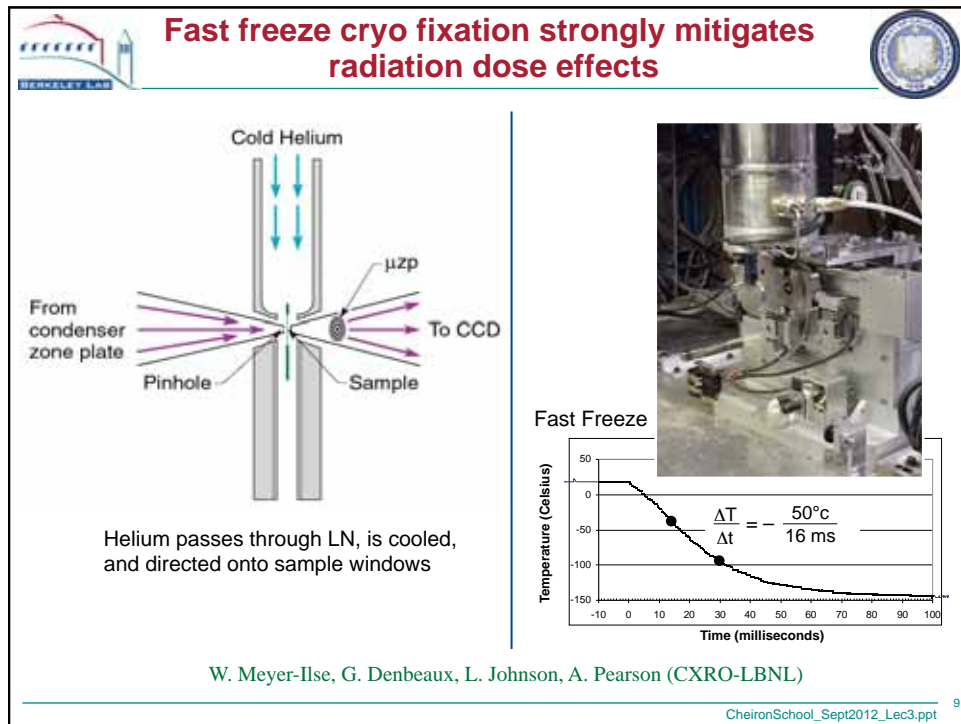
Cr/Si test pattern (Cr L₃ @ 574 eV)
 (2000 X 2000, 10⁴ ph/pixel)

Novel zone plates for specific functionality

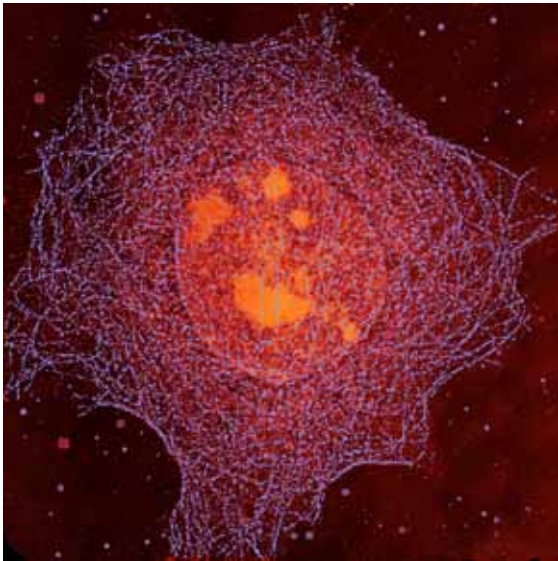


Courtesy of Anne Sakdinawat, UC Berkeley





Bending magnet radiation used with a soft x-ray microscope to form a high resolution image of a whole, hydrated mouse epithelial cell



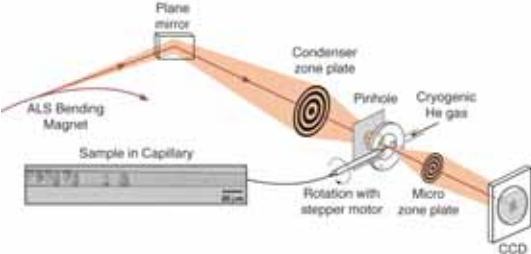
$h\nu = 520 \text{ eV}$
 $32 \mu\text{m} \times 32 \mu\text{m}$
 Ag enhanced Au labeling of the microtubule network, color coded blue.
 Cell nucleus and nucleoli, moderately absorbing, coded orange.
 Less absorbing aqueous regions coded black.
 W. Meyer-Ilse et al.
 J. Microsc. 201, 395 (2001)

Courtesy of C. Larabell and W. Meyer-Ilse (LBNL)

CheironSchool_Sept2012_Lec3.ppt 11

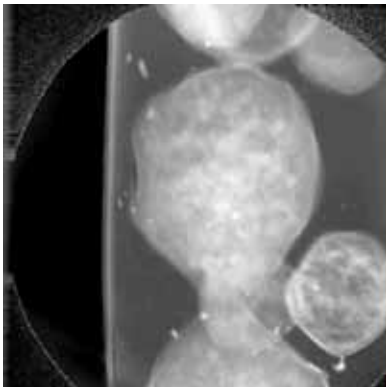
Bio-nanotomography for 3D imaging of cells

Nanotomography of Cryogenic Fixed Cells



Courtesy of G. Schneider (BESSY)
Surf. Rev. Lett. 9, 177 (2002)

Soft X-Ray Nanotomography of a Yeast Cell




$\lambda = 2.4 \text{ nm}$


Courtesy of C. Larabell (UCSF & LBNL)
 and M. LeGros (LBNL)

UCSF NCXT

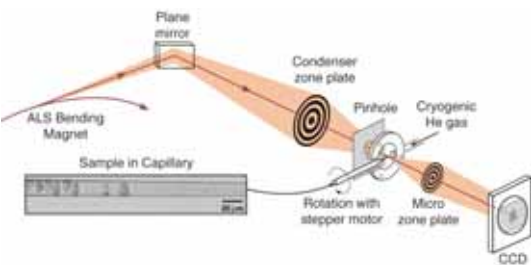
CheironSchool_Sept2012_Lec3.ppt 12



Bio-nanotomography for 3D imaging of cells

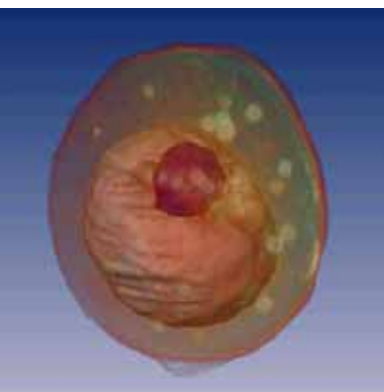


Nanotomography of Cryogenic Fixed Cells




$\lambda = 2.4 \text{ nm}$ (517 eV)
 $\Delta r = 35 \text{ nm}$
 $N = 320$
 $NA = 0.034$
 $D = 45 \text{ }\mu\text{m}$
 $f = 650 \text{ }\mu\text{m}$
 $\sigma = 0.64$
 Resolution = 60 nm


Soft X-Ray Nanotomography of a Yeast Cell




$\lambda = 2.4 \text{ nm}$

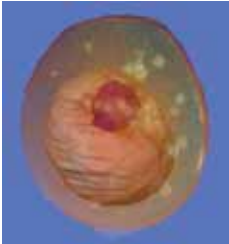
Courtesy of C. Larabell (UCSF & LBNL) and M. LeGros (LBNL)


CheironSchool_Sept2012_Lec3.ppt 13

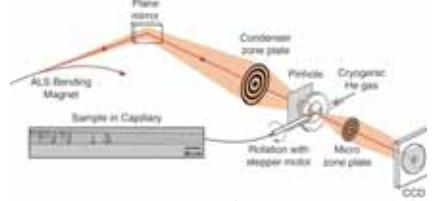


Small DOF limits resolution for thick samples





C. Larabell and M. LeGros,
Molec. Bio. Cell **15**, 957 (2004)

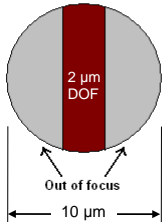


Lateral Resolution = $\frac{k_1 \lambda}{NA} = 2k_1 \Delta r = \cancel{28 \text{ nm}} 60 \text{ nm}$

Depth of field = $\quad \quad \quad = 2 \text{ }\mu\text{m}$

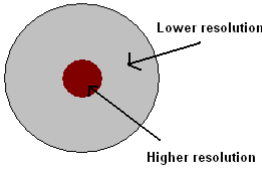
Each projection image

In focus region





10 μm

Reconstructed image

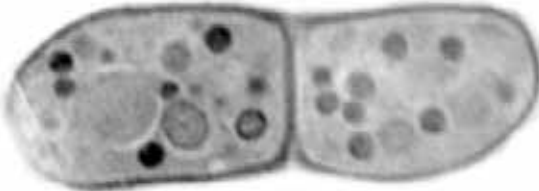


Courtesy of Anne Sakdinawat (LBNL & UCB.)
CheironSchool_Sept2012_Lec3.ppt 14

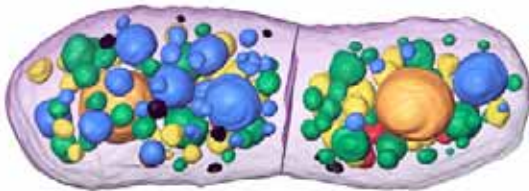


Nanoscale 3-D biotomography

Mother daughter yeast cells just before separation





2-D slice from 3-D Tomogram. Images every 2°, 180° data set, several minutes. $\Delta r = 45$ nm



Color coding identifies subcellular components by their x-ray absorption coefficients


Courtesy of Carolyn Larabell, UCSF/LBNL.

CheironSchool_Sept2012_Lec3.ppt 15



Applications of soft x-ray microscopy

Biotomography at 60 nm resolution



- Cryofixation
- 2° angular intervals
- Depth of focus limits resolution
- New XM-2 dedicated to biological applications, will become major facility worldwide to draw biologists to this evolving capability


Courtesy of C. Larabell (UCSF & LBNL)

UCSF NCXT

CheironSchool_Sept2012_Lec3.ppt 16

BESSY **High resolution (29 nm), 3D image of a mouse cell by soft x-ray tomography**

2D slice from 3D data set



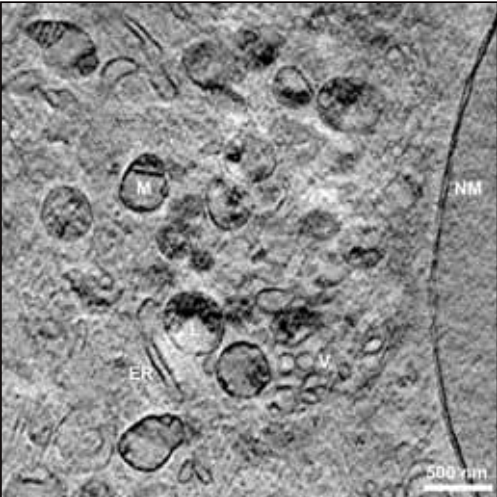
517 eV (2.4 nm)
 $\Delta r = 25$ nm,
1° intervals, $\pm 60^\circ$
29 nm nuclear
double membrane.

Courtesy of
Gerd Schneider, BESSYII
and James McNally, NIH.

CheironSchool_Sept2012_Lec3.ppt 17

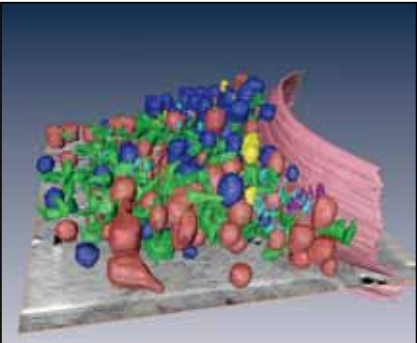
BESSY **High resolution (29 nm), 3D image of a mouse cell by soft x-ray tomography**

2D slice from 3D data set




Details: 517 eV (2.4 nm)
 $\Delta r = 25$ nm, 1° intervals, $\pm 60^\circ$.
Note 29 nm nuclear membrane.

3D rendering




Courtesy of Gerd Schneider, BESSYII and James McNally, NIH.

CheironSchool_Sept2012_Lec3.ppt 18

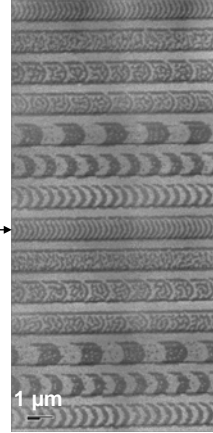


Magnetic x-ray microscopy using x-ray magnetic circular dichroism (XMCD)




Magnetic X-Ray Microscopy

- High spatial resolution in transmission
- Bulk sensitive (thin films)
- Complements surface sensitive PEEM
- Good elemental sensitivity
- Good spin-orbit sensitivity
- Allows applied magnetic field
- Insensitive to capping layers
- In-plane and out-of-plane measurements




Courtesy of P. Fischer, (MPI, Stuttgart) and G. Denbeaux (CXRO/LBNL)

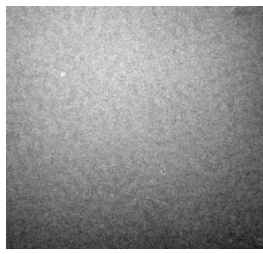
19
CheironSchool_Sept2012_Lec3.ppt



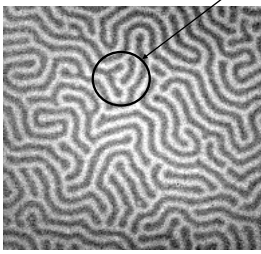
Magnetic domains imaged at different photon energies



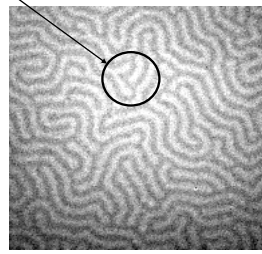
FeGd Multilayer



$\hbar\omega = 704$ eV
below Fe L-edges



$\hbar\omega = 707.5$ eV
Fe L₃-edge





$\hbar\omega = 720.5$ eV
Fe L₂-edge

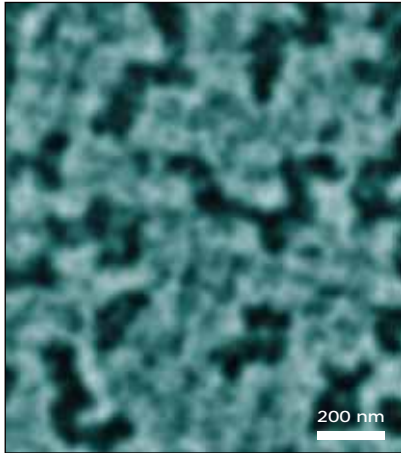
Contrast reversal

P. Fischer, T. Eimüller, M. Koehler (U. Würzburg)
S. Tsunashima (U. Nagoya) and N. Tagaki (Sanyo)
G. Denbeaux, L. Johnson, A. Pearson (CXRO-LBNL)

20
CheironSchool_Sept2012_Lec3.ppt



Magnetic recording of nanomagnetic patterns to 15 nm spatial resolution





CoCrPt alloy
Co L₃-edge at 778 eV
(1.59 nm)

Courtesy of Peter Fischer (LBNL)

P. Fischer et al., *Mat. Today* 9, 26 (2006).

21
CheironSchool_Sept2012_Lec3.ppt




Time resolved studies of vortex dynamics in patterned permalloy thin films


Pump and Probe setup requires:

- Pump: Current pulse to "pump" sample
- Probe: X-ray pulses (70ps) from ALS 2 Bunch mode
- Perfect repeatability of dynamics


Sample:
50 nm thick 2μm x 4μm permalloy (Ni₈₀Fe₂₀)
100nm thick gold waveguide
(ΔI along waveguide generates field to pump sample)




Before Pump (t=0)



t = +1 ns

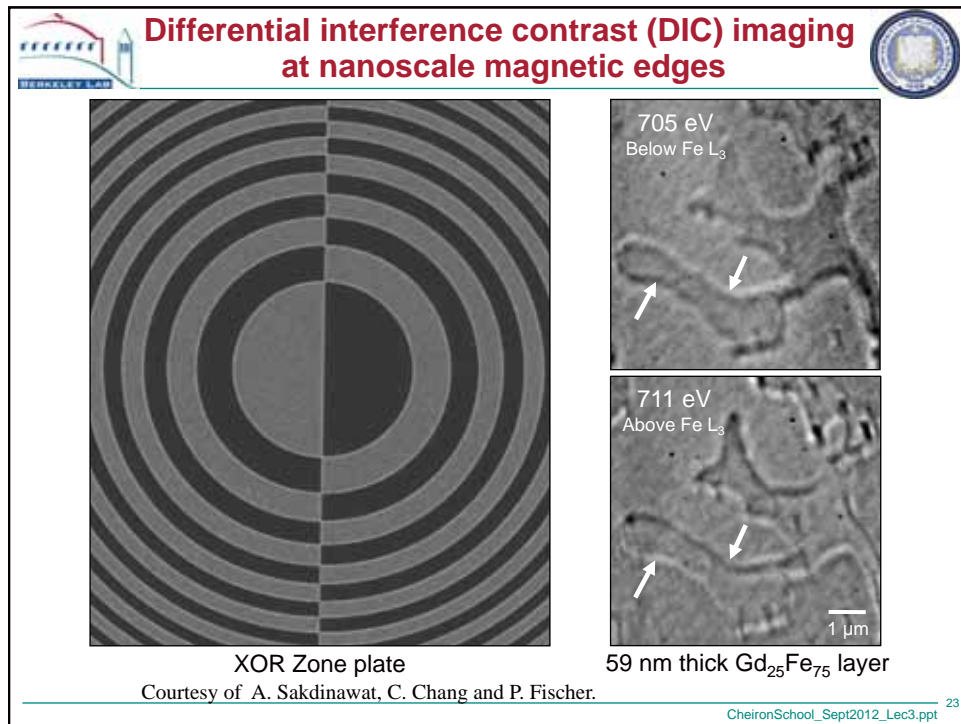


t = +1.6 ns



B.L. Mesler, P. Fischer, W. Chao, E. H. Anderson, D.H. Kim J. Vac. Sci. Technol. B 25, 2598 (2007).

22
CheironSchool_Sept2012_Lec3.ppt



Environmental Consequences of Portland cement

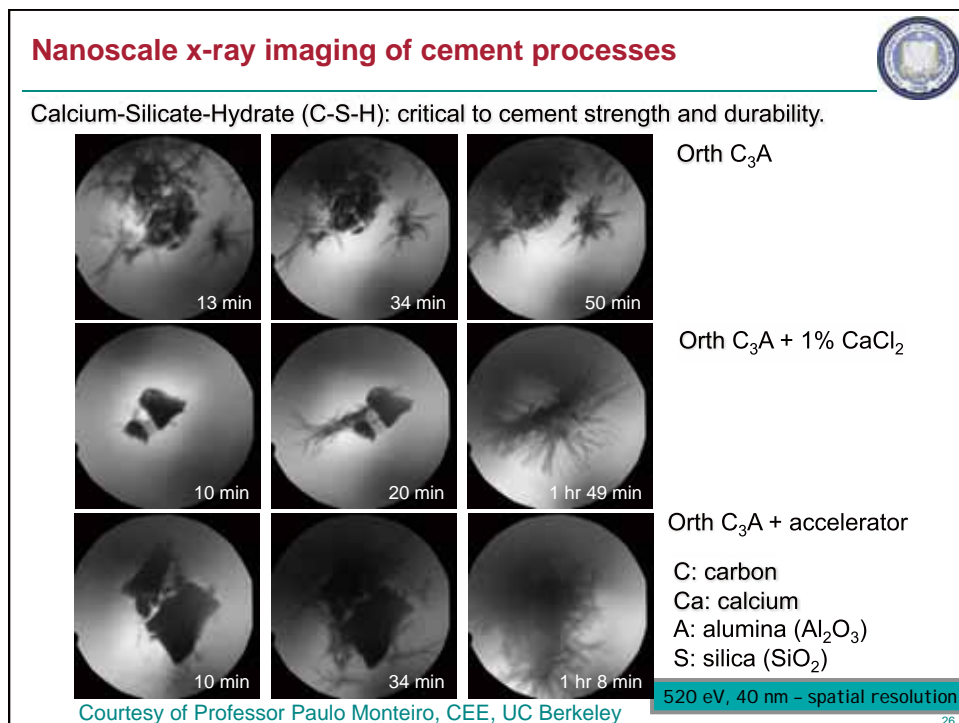
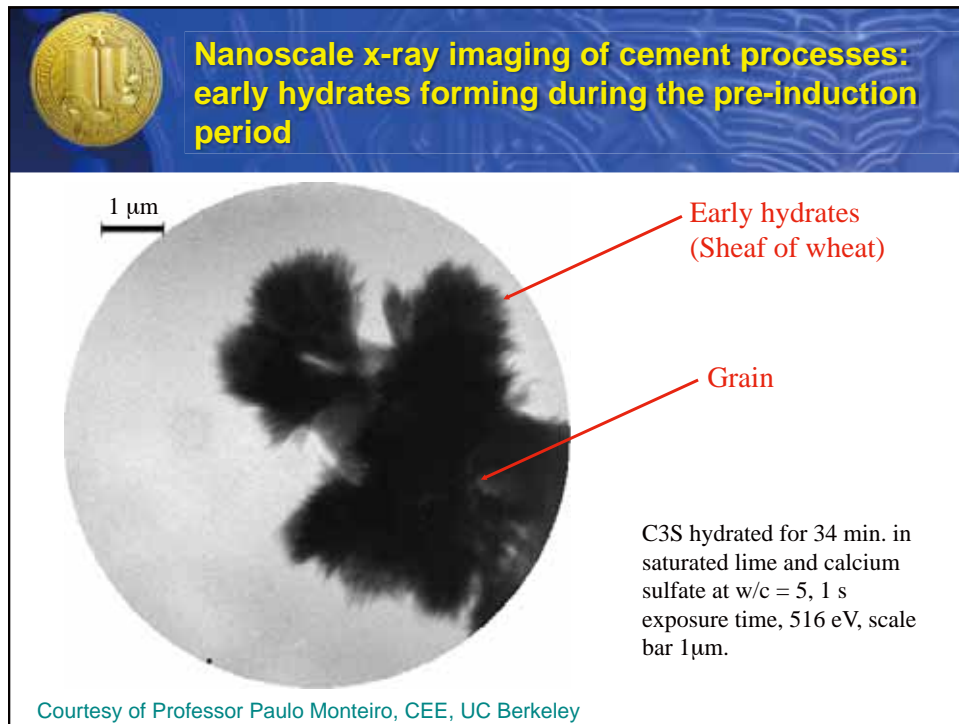
1.5 billion ton of cement

Generates 1.5 billion ton of CO_2

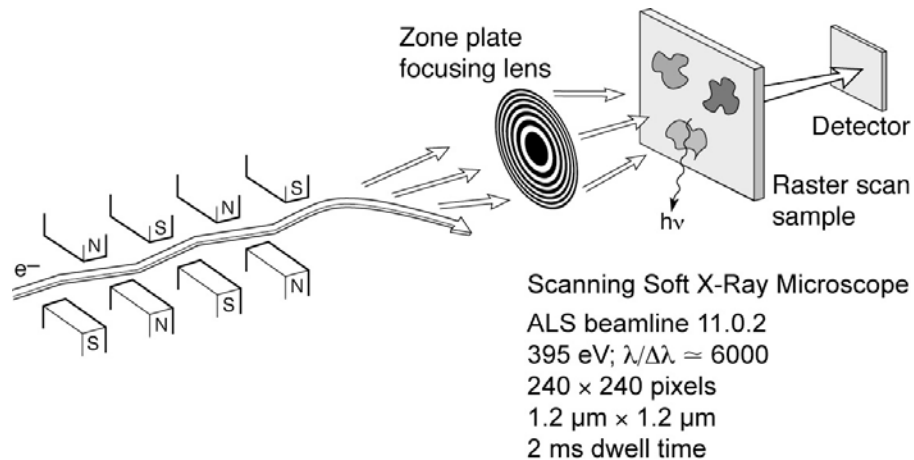
Responsible for 7% CO_2 production in the world

Problem!

Courtesy of Professor Paulo Monteiro, CEE, UC Berkeley



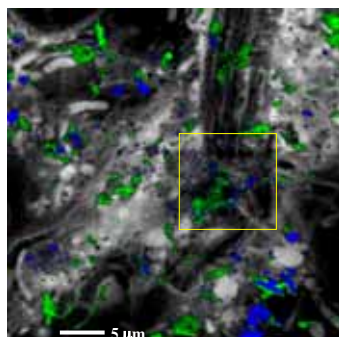
Spectromicroscopy: high spatial and high spectral resolution of surface and thin films



Ch09_F40a_Feb2010.ai

CheironSchool_Sept2012_Lec3.ppt 27

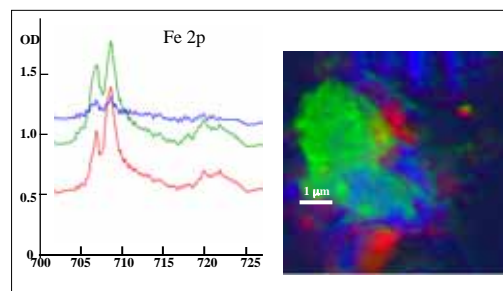
Biofilm from Saskatoon River



Protein (gray), Ca, K

RESULTS

- Ni, Fe, Mn, Ca, K, O, C elemental map, (there was no sign of Cr.)
- Different oxidation states for Fe and Ni

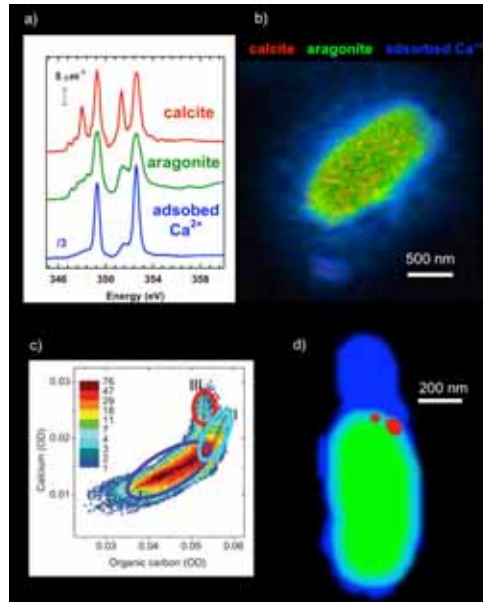


Different oxidation states (minerals) found for Fe & Ni

Tohru Araki, Adam Hitchcock (McMaster University)
Tolek Tyliczszak, LBNL
Sample from: John Lawrence, George Swerhone (NWRI-Saskatoon), Gary Leppard (NWRI-CCIW)

CheironSchool_Sept2012_Lec3.ppt 28

A. Hitchcock, McMaster U.



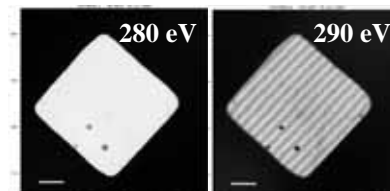
CheironSchool_Sept2012_Lec3.ppt 29



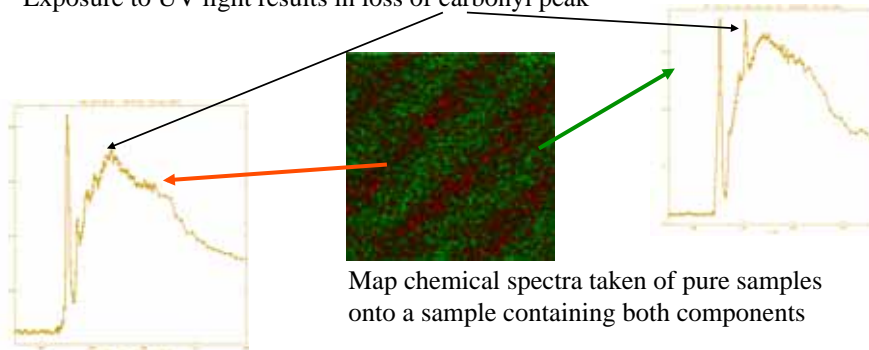
Patterned polymer photoresists



M.K. Gilles, R. Planques, S.R. Leone
LBNL
Samples from B. Hinsberg, F. Huele
IBM Almaden



Exposure to UV light results in loss of carbonyl peak



Courtesy of Mary Gilles, LBNL

CheironSchool_Sept2011_Lec3.ppt 30

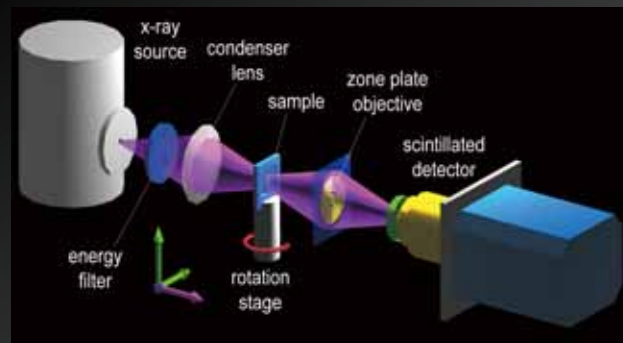
Hard x-ray zone plate microscopy



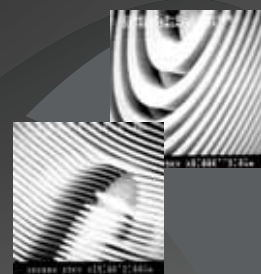
- Shorter wavelengths, potentially better spatial resolution and greater depth-of-field.
- Less absorption (β); phase shift (δ) dominates, higher efficiency.
- Thicker structures required (e.g., zones), higher aspect ratios pose nanofabrication challenges.
- Contrast of nanoscale samples minimal; will require good statistics, uniform background, dose mitigation.

CheironSchool_Sept2012_Lec3.ppt 31

nanoXCT: Schematic and Challenges



X-ray Zone-plate Lens



Challenges for achieving nm scale resolution:

- High resolution objective lens: limiting the ultimate resolution
- High numerical aperture condenser lens:
- Detector: high efficiency for lab. source and high speed for synchrotron sources
- Precision mechanical system

Courtesy of Wenbing Yun and Michael Feser, Xradia

32

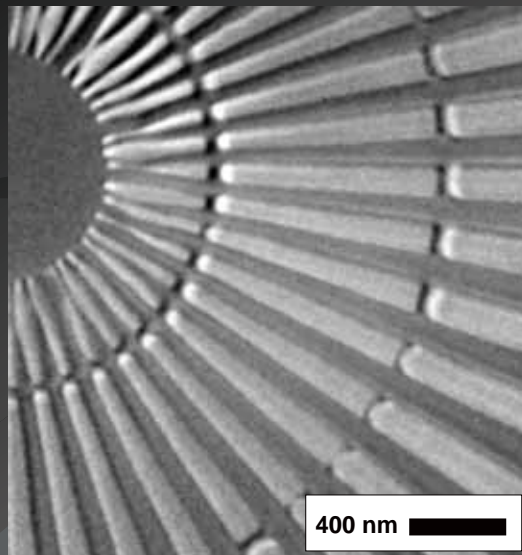
Xradia nanoXCT: Sub-25 nm Hard X-ray Image

Xradia Resolution Pattern

- 50 nm bar width
- 150 nm thick Au
- 8keV x-ray energy
- 3rd diffraction order

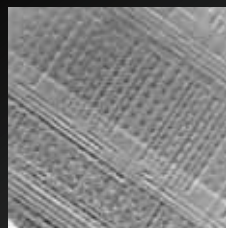
F. Duewer, M. Tang,
G. C. Yin, W. Yun,
M. Feser, et al.

Xradia nano-XCT
8-50S installed at
NSRRC, Taiwan

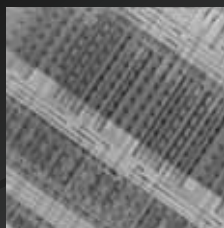


33

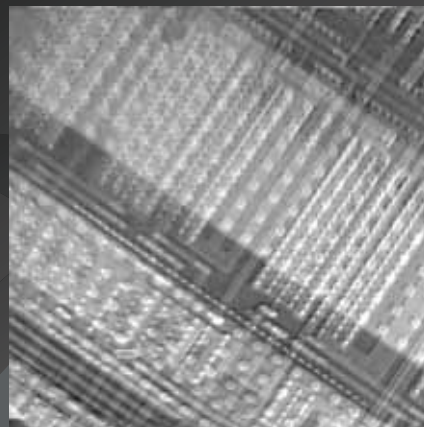
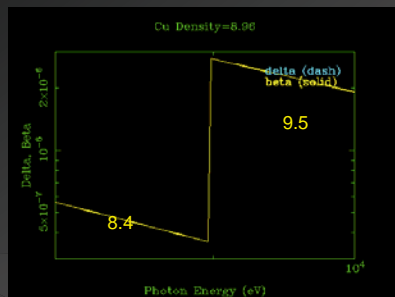
Elemental contrast by tuning energy across the copper absorption edge (Guan-Chian Yin *et al*)



8.4 keV

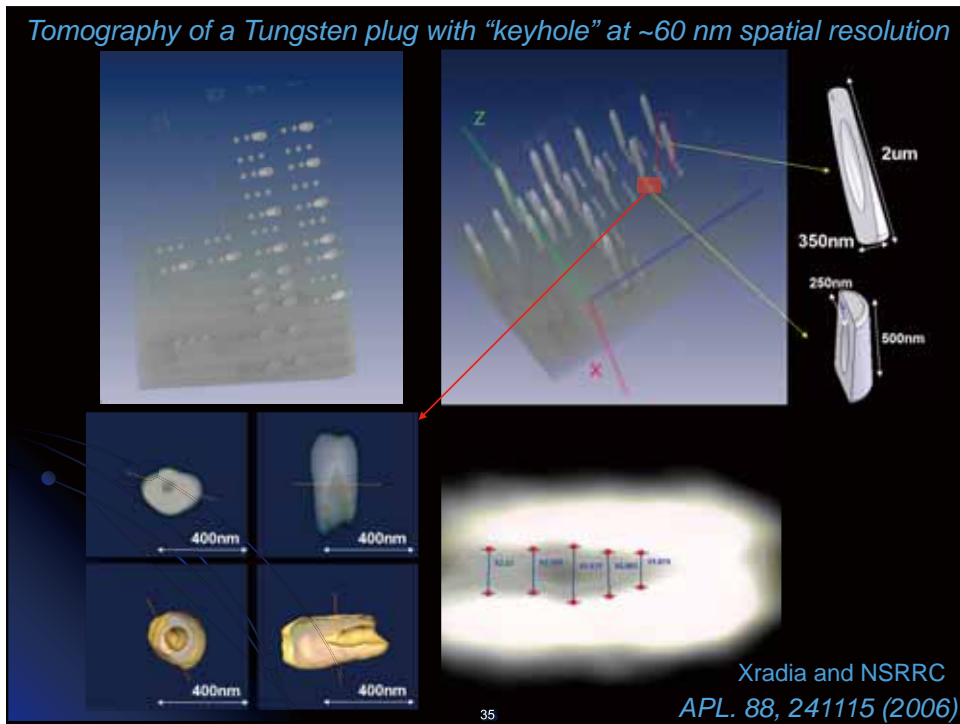


9.5 keV

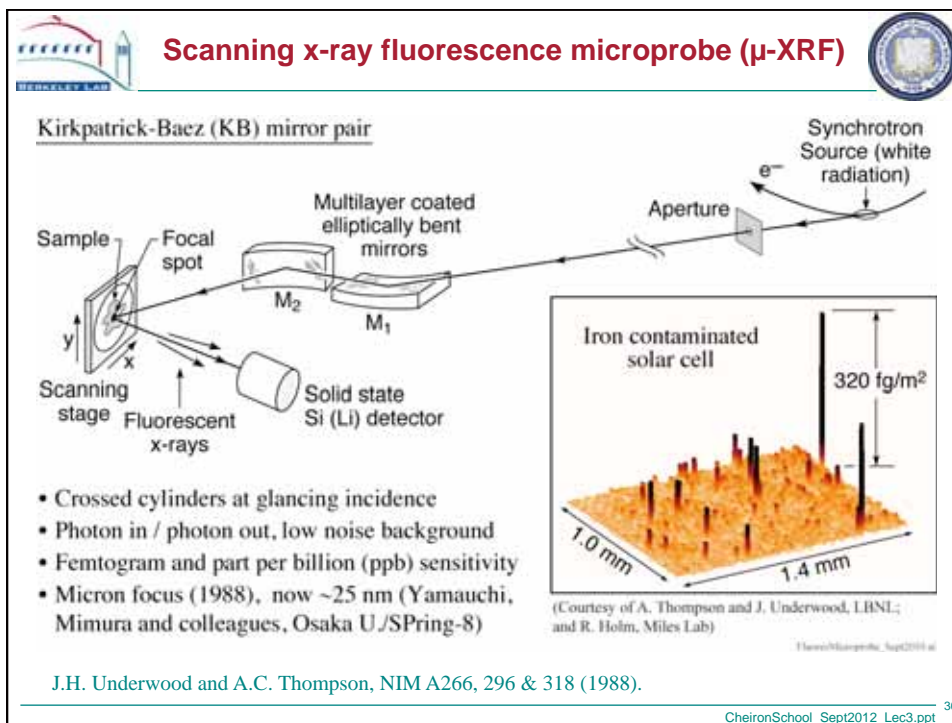


Intensity difference between
E = 8.4 keV and 9.5 keV

34

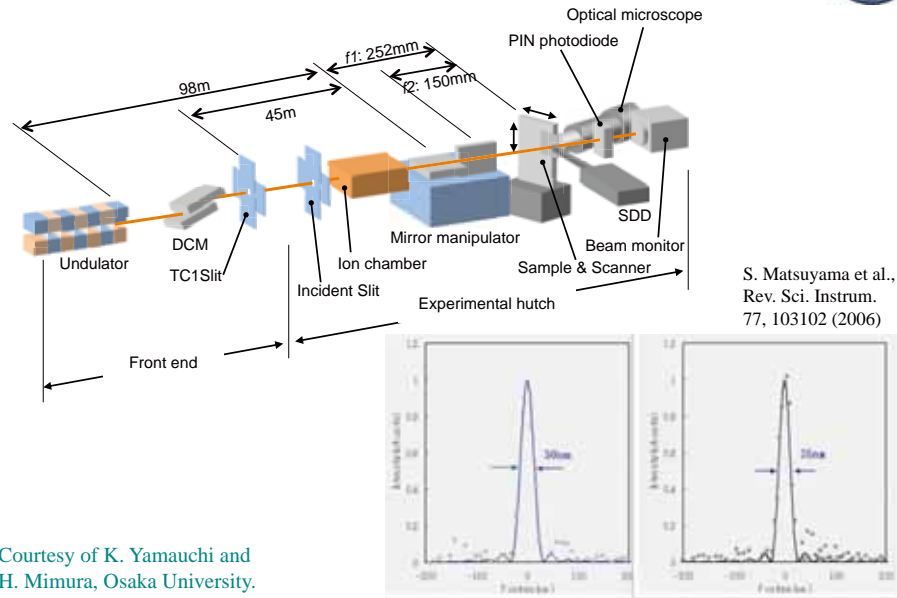


35



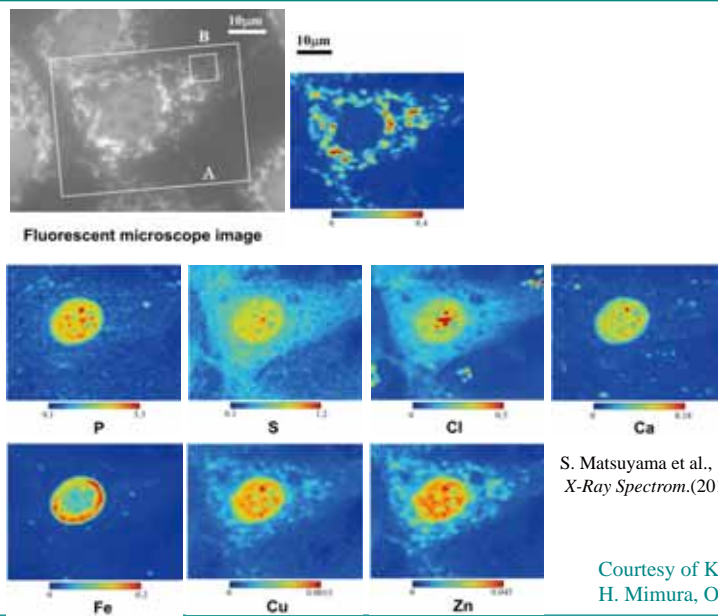
36

X-ray microprobe at SPring-8

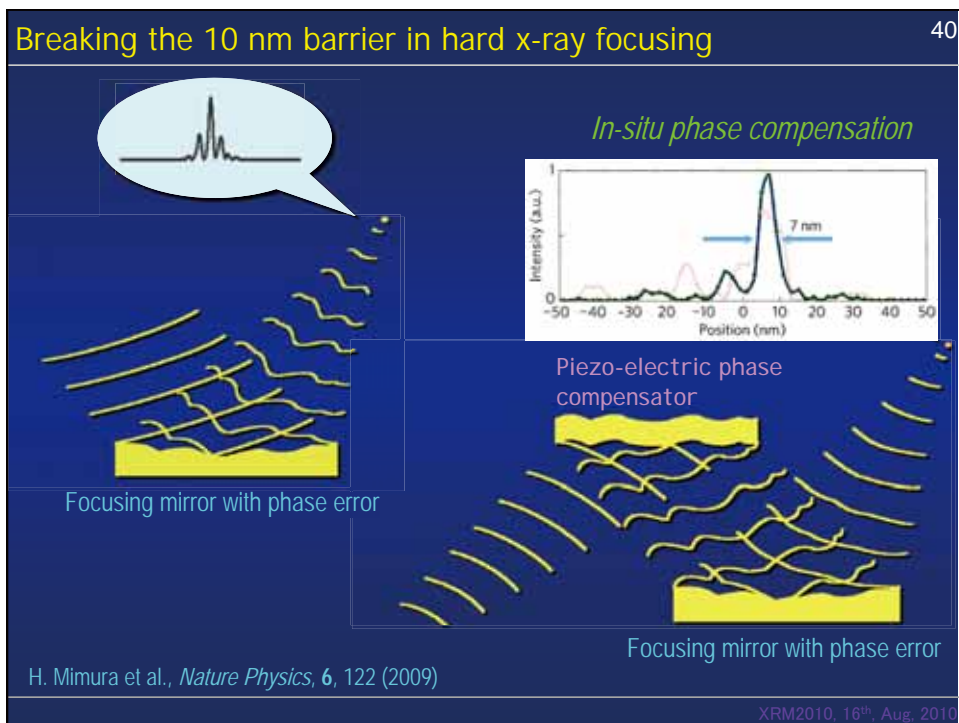
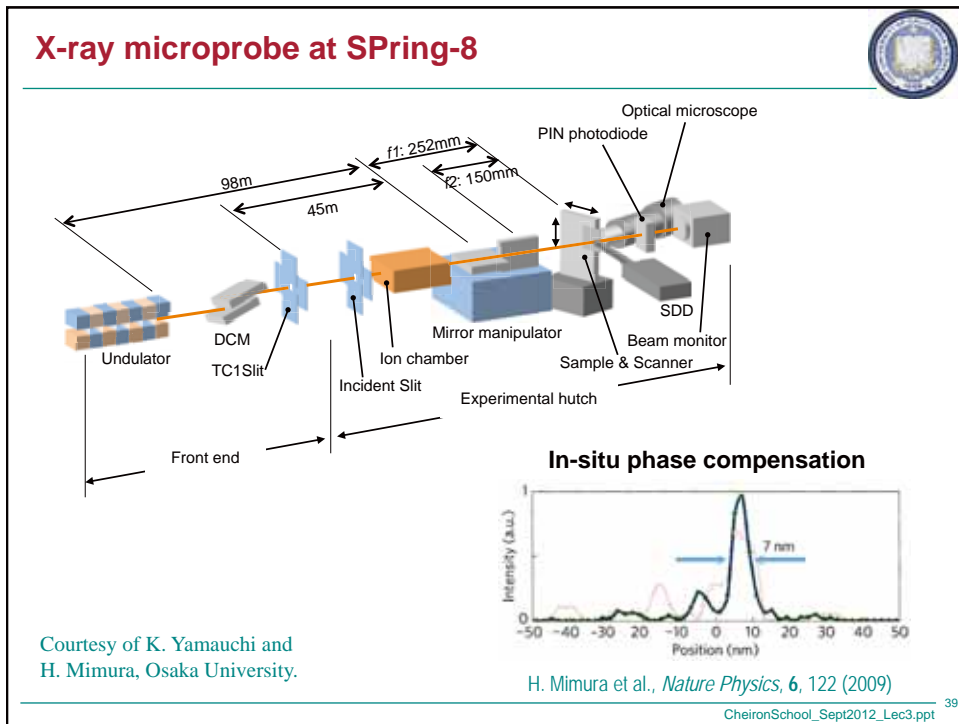


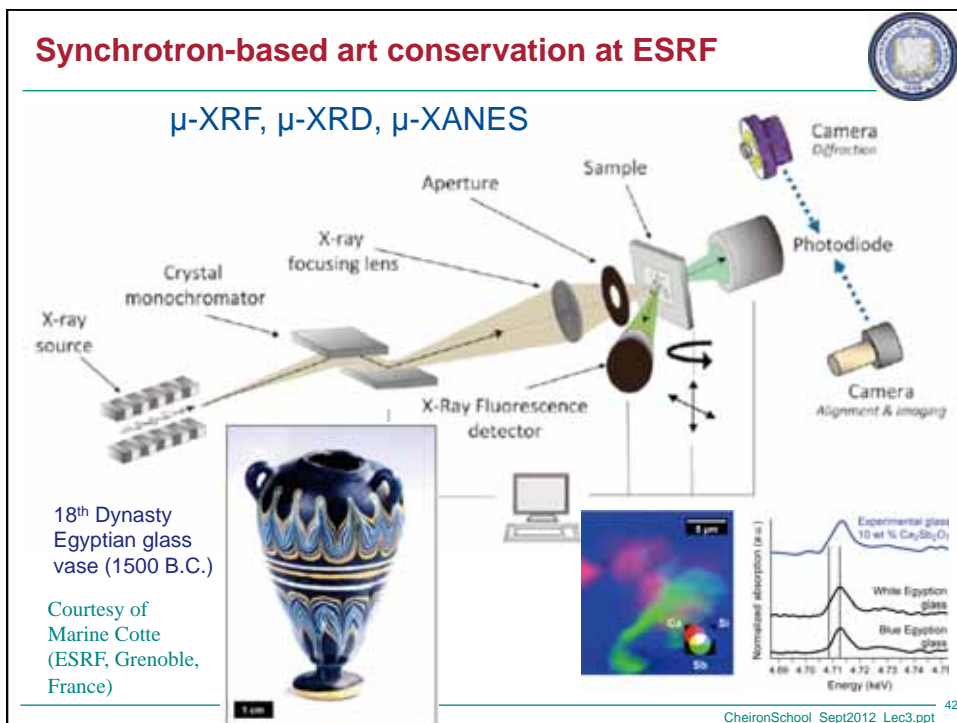
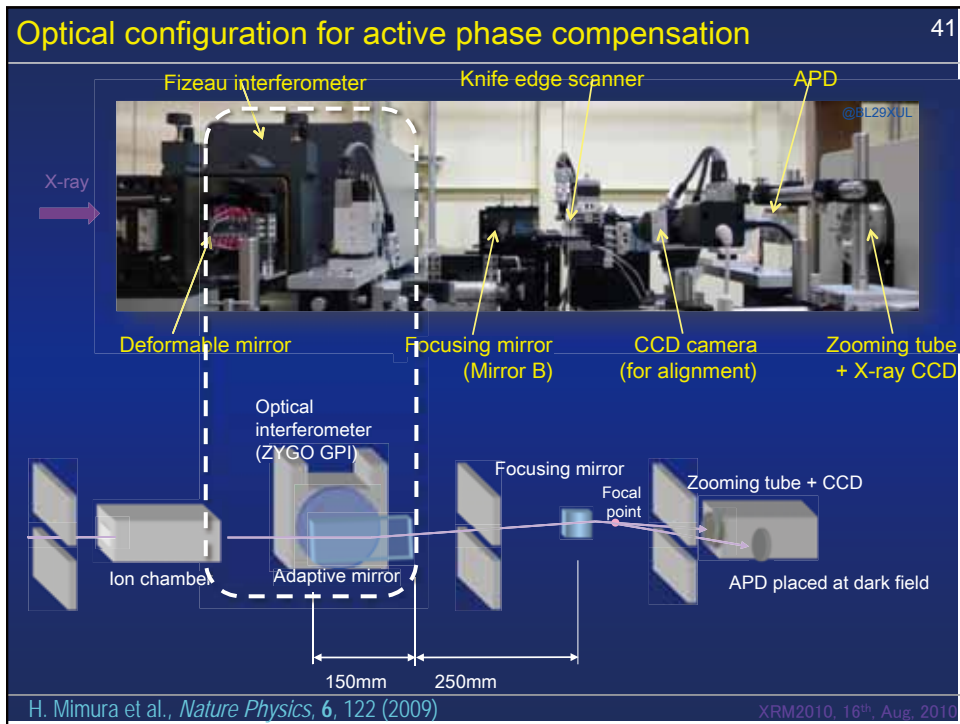
CheironSchool_Sept2012_Lec3.ppt 37

Sub-cellular elemental analysis using the hard x-ray fluorescence microprobe at SPring-8

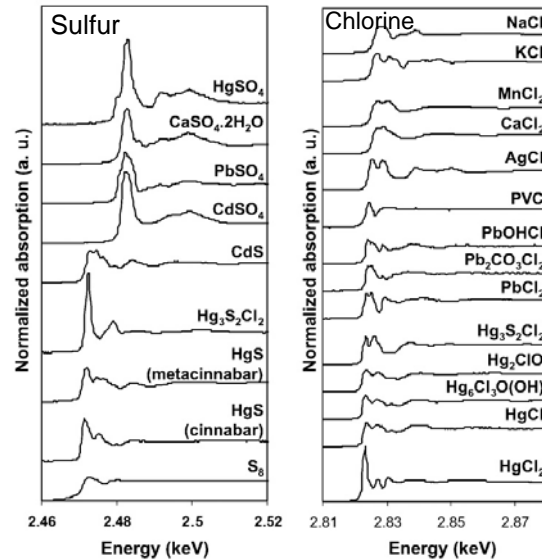


CheironSchool_Sept2012_Lec3.ppt 38





Examples of μ -XANES K-edge spectra occurring in art materials

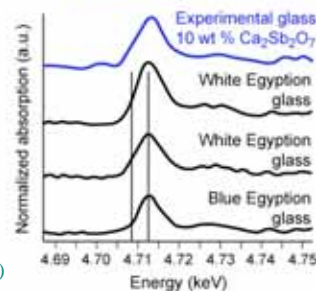
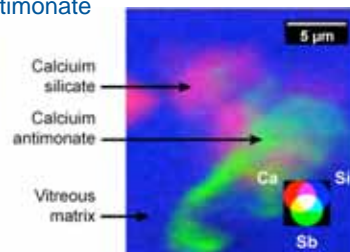


Courtesy of Marine Cotte (ESRF, Grenoble, France)

CheironSchool_Sept2012_Lec3.ppt 43

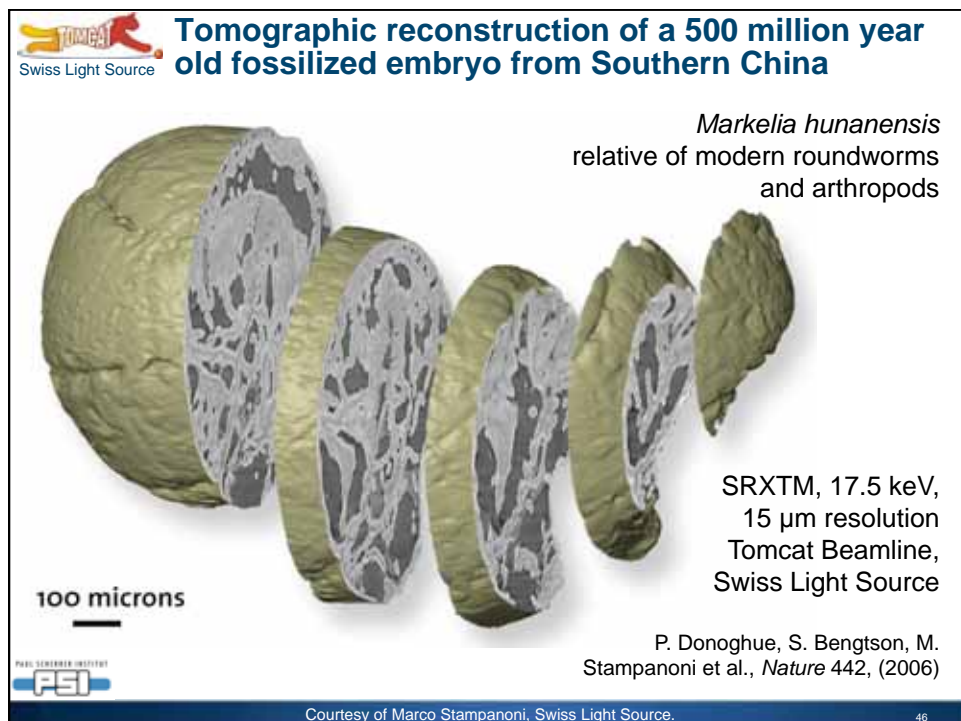
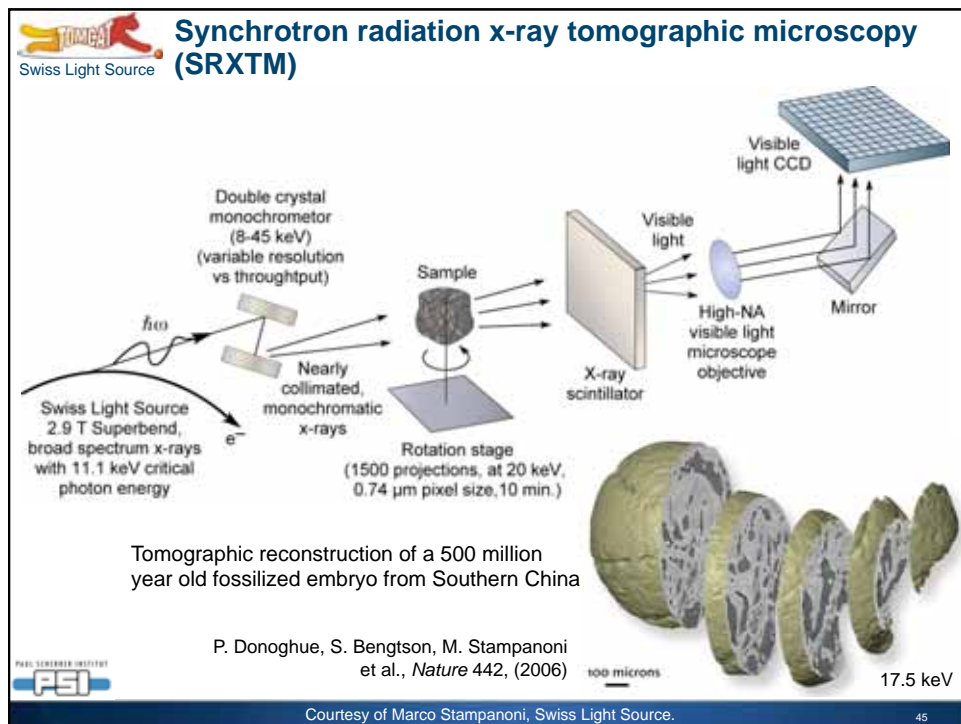
18th Dynasty Egyptian glass vase studied for an understanding of color and opaqueness in antiquity

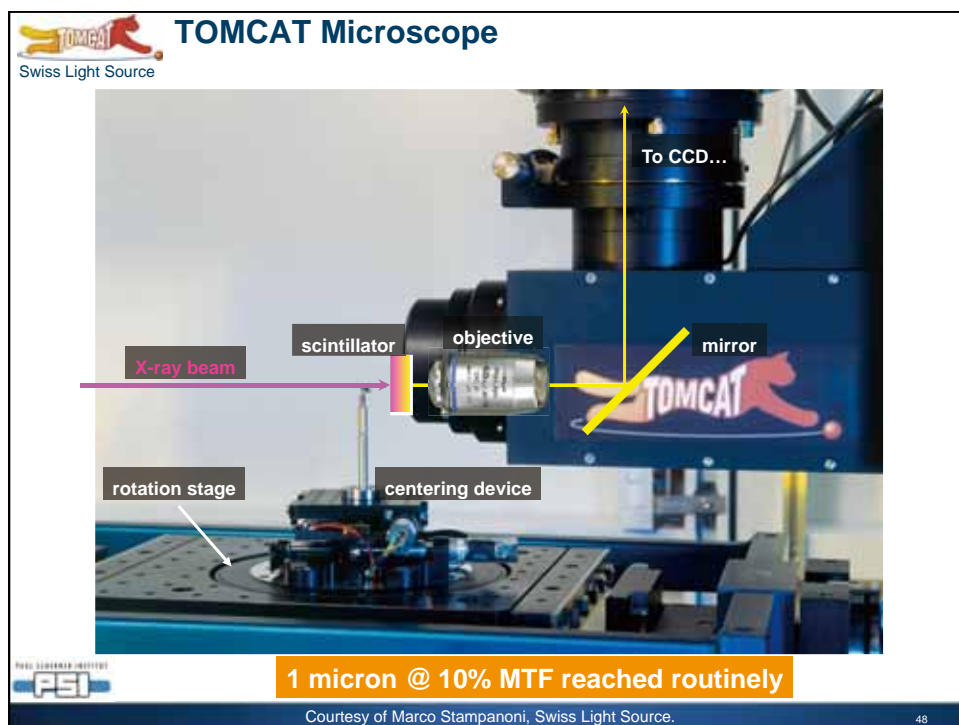
1st production of glass objects Egypt (1500 B.C.),
opaque, colored, nanoscale calcium antimonate

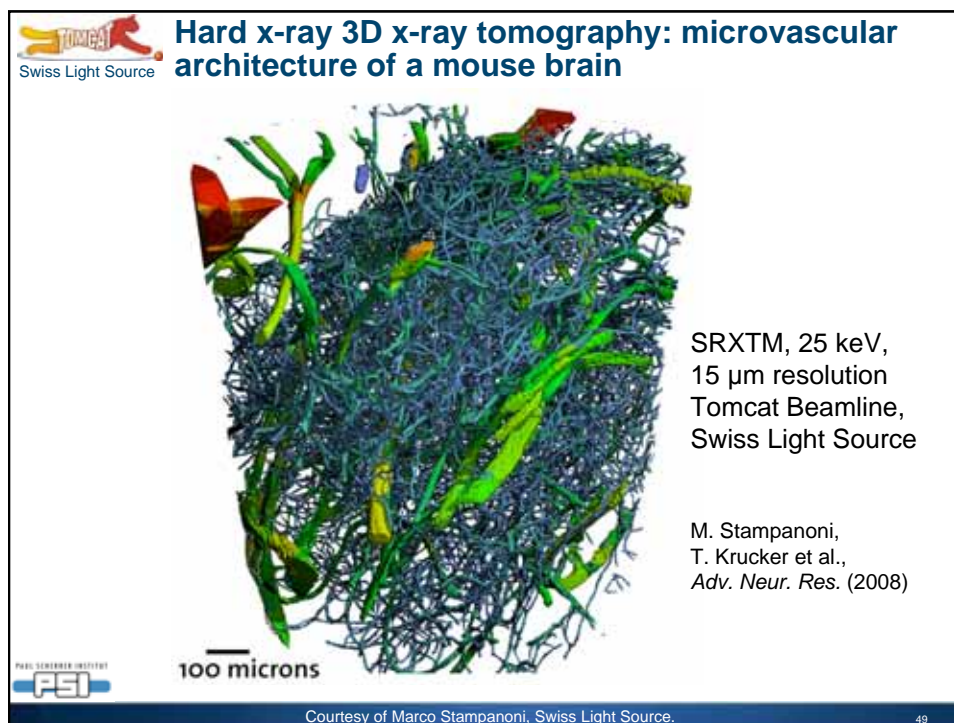


Courtesy of Marine Cotte (ESRF, Grenoble, France)

CheironSchool_Sept2012_Lec3.ppt 44

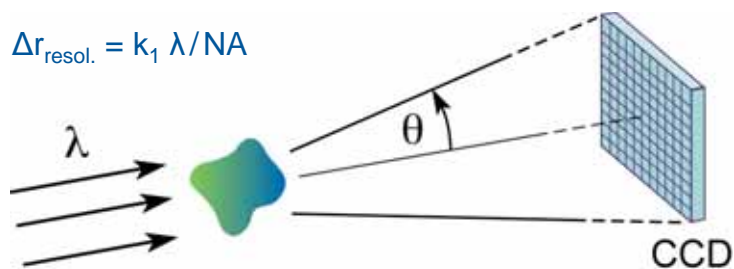




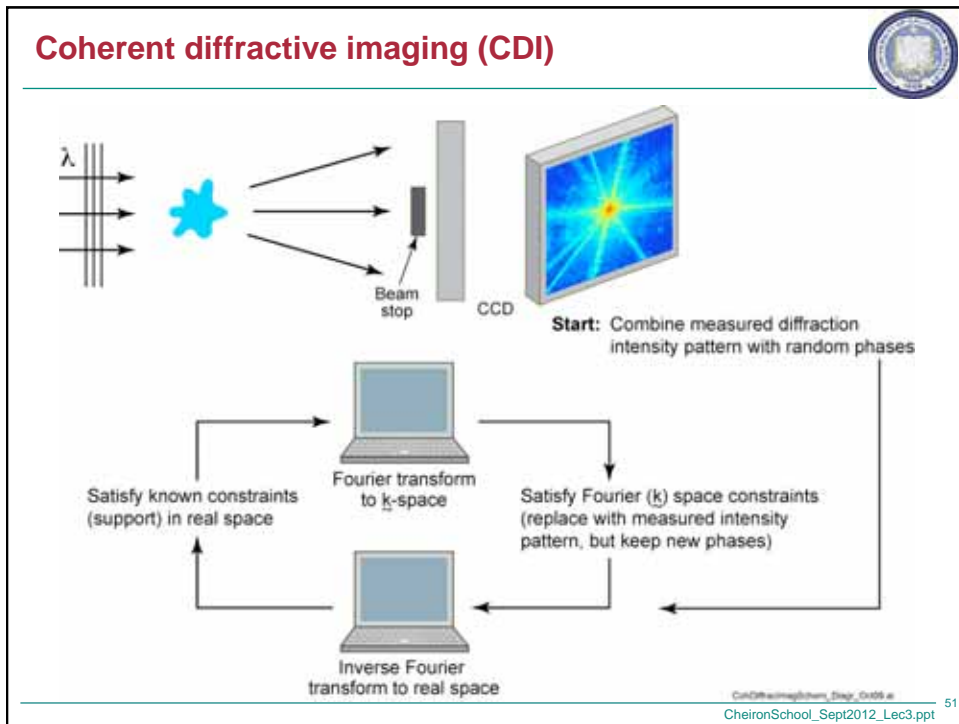


A lens is not necessarily required

$$\Delta r_{\text{resol.}} = k_1 \lambda / \text{NA}$$



“Lensless” coherent diffraction imaging (CDI) is being aggressively pursued.



Coherent diffractive imaging (CDI) examples

Femtosecond diffractive imaging with a free electron laser

Flash FEL, $\lambda = 32$ nm (39 eV)
25 fsec, 10^{12} photons/pulse
62 nm resolution
Chapman, et al. Nature Physics (2006)

CDI with laboratory scale high harmonic generation (HHG)

HHG, $n = 27$, $\lambda = 29$ nm (43 eV)
94 nm spatial resolution
Sandberg, et al. PNAS (2008)

Synchrotron based CDI of 100 nm Au spheres

FIG. 1 (color online). (a) Schematic sketch of the coherent diffractive imaging setup with multi-focused illumination, the scanning electron micrograph of gold particles (diameter ~ 100 nm) deposited on a Si_3N_4 membrane. (b) Diffraction pattern (logarithmic scale) recorded of the single gold particles pointed to by the green circle and illuminated by a hard x-ray beam with lateral dimensions of about 100×100 nm². The measured momentum transfer, both in horizontal and vertical directions, is up to $1/100$ nm⁻¹.

FIG. 2. (a) Two individual reconstructions of the gold particle using the HIO algorithm, a left- and a right-handed one. To find the average particle shape from a series of reconstructions only random initial phases, the right-handed reconstructions can be inverted and averaged together with the left-handed ones to Reconstructed projected electron density of the gold nano-particle shown in (b). (c) Horizontal section through the center of the particle shown in (b). The error bars indicate one standard deviation for the series of independent reconstructions.

Synchrotron CDI of Au particles
 $\lambda = 0.083$ nm (15 keV),
5 nm "resolution"
Schroer, et al. PRL (2008)

Synchrotron based CDI of a freeze dried yeast cell

CDI
ALS/9.0.1
 $\lambda = 1.66$ nm (750 eV)

STXM
NSLS/X1
 $\lambda = 2.3$ nm (540 eV)
42 nm resolution

Tilted 3°

Tilted 4°

30 nm fine features
Shapiro, et al. PRL (2005)

52

BESSY **Lensless imaging of magnetic nanostructures by x-ray spectro-holography**

The diagram illustrates the experimental setup for lensless imaging. X-rays pass through a 20 µm pinhole and illuminate a mask and sample. The mask consists of an Au mask, a SiN_x membrane, and a Magnetic film. The sample is a magnetic nanostructure. The resulting STXM image shows a complex pattern of magnetic domains with a 1.5 µm scale bar. A CCD detector captures the diffracted X-rays, showing a central spot and surrounding rings. An SEM image of the mask shows a circular hole with a 2 µm scale bar.

S. Eisebitt, J. Lüning, W.F. Schlott, M. Lörger, O. Hellwig, W. Eberhardt & J. Stöhr / *Nature*, 16 Dec 2004

CheironSchool_Sept2012_Lec3.ppt 53

Lectures online at www.youtube.com

The image shows the cover of the book "SOFT X-RAYS AND EXTREME ULTRAVIOLET RADIATION: Principles and Applications" by David Attwood, published by Amazon.com. An arrow points from the book cover to a photograph of the UC Berkeley Campanile tower.

UC Berkeley
www.coe.berkeley.edu/AST/sxreuv
www.coe.berkeley.edu/AST/srms
www.coe.berkeley.edu/AST/sxr2009

CheironSchool_Sept2012_Lec3.ppt 54